Cell Communication and Signaling

RESEARCH Open Access

Menin-driven mTOR signaling sustains taxane resistance in CRPC and reveals a targetable vulnerability for combination therapy

Ipek Bulut[1,2], Buse Cevatemre[1,3], Neslihan Yuksel-Catal[2], Hamzah Syed[1,3], Tamer Onder[1,3] and Ceyda Acilan[1,3*]

Abstract

Prostate cancer (PC) progression is predominantly driven by androgen signaling, making androgen deprivation therapy (ADT) the standard treatment. However, the transition to castration-resistant prostate cancer (CRPC) significantly reduces ADT efficacy. While taxanes such as docetaxel (Dtx) and cabazitaxel (Cbz) are widely employed, therapeutic resistance remains a major clinical obstacle. To address this, we established docetaxel-resistant CRPC models and performed an epigenetic drug screen, identifying MLL-Menin and MLL-WDR5 inhibitors as potent agents capable of restoring taxane sensitivity through G_2/M arrest and apoptosis induction. Functional depletion of Menin (MEN1) revealed its critical role in sustaining chemoresistance, selectively impairing proliferation in resistant cells, and preventing resistance emergence in parental lines.

Integrative transcriptomic (RNA-seq) and epigenomic (CUT&RUN-seq) analyses suggested that Menin may play a regulatory role in mTOR signaling and E2F target pathways. Menin binding to the promoters of mTOR and Cyclin D1 was confirmed, and rescue experiments further validated its regulatory role. Analysis of TCGA datasets demonstrated co-expression of MEN1 and mTOR in advanced metastatic PC, supporting clinical relevance. Moreover, combination treatment with the mTOR inhibitor Torin-1 and docetaxel synergistically enhanced therapeutic response in Menin-depleted resistant cells. MEN1 knockdown also abrogated tumor growth in vivo. These findings identify Menin as one of the key mediator of taxane resistance in CRPC through the regulation of mTOR. Targeting Menin, alone or in combination with mTOR inhibition, represents a promising strategy to overcome resistance and improve therapeutic outcomes in taxane-refractory PC.

Introduction

Prostate cancer (PC) is the second most common cause of cancer-related mortality among men, with an estimated 1.4 million new cases reported each year [1]. Removal of the prostate gland (prostatectomy) and radiotherapy are considered initial therapeutic protocols [2], followed by castration (androgen deprivation) therapy, either reducing androgen synthesis or blocking the androgen receptor (AR) activity [3]. Despite the castration therapy, the localized tumors may develop metastatic features, allowing cells to migrate to other areas of the body (bones, lymph nodes, lungs, or brain), and the

*Correspondence:
Ceyda Acilan
cayhan@ku.edu.tr
[1]Koc University Research Center for Translational Medicine, Istanbul, Turkey
[2]Koc University Graduate School of Health Sciences, Istanbul, Turkey
[3]Koc University School of Medicine, Istanbul, Turkey

© The Author(s) 2025. **Open Access** This article is licensed under a Creative Commons Attribution-NonCommercial-NoDerivatives 4.0 International License, which permits any non-commercial use, sharing, distribution and reproduction in any medium or format, as long as you give appropriate credit to the original author(s) and the source, provide a link to the Creative Commons licence, and indicate if you modified the licensed material. You do not have permission under this licence to share adapted material derived from this article or parts of it. The images or other third party material in this article are included in the article's Creative Commons licence, unless indicated otherwise in a credit line to the material. If material is not included in the article's Creative Commons licence and your intended use is not permitted by statutory regulation or exceeds the permitted use, you will need to obtain permission directly from the copyright holder. To view a copy of this licence, visit http://creativecommons.org/licenses/by-nc-nd/4.0/.

disease is referred to as castration-resistant prostate cancer (CRPC) [4]. Taxanes such as docetaxel or cabazitaxel are the chemotherapy options for CRPC [5]; however, the therapy response is compromised by the emergence of drug resistance. Therefore, revealing the molecular mechanisms underlying drug resistance is essential for developing strategies to restore sensitivity to taxane-based treatments.

Numerous research groups, including ours, have extensively investigated the mechanisms underlying taxane resistance, which include the upregulation of Multidrug resistance 1 (MDR1) [6], microtubule mutations [7], drug-metabolizing enzymes [8], anti-apoptotic pathways [9, 10], epithelial to mesenchymal transition (EMT) [11], dysregulation of centrosomal kinases and cell cycle checkpoints [12, 13], non-coding RNA's [14], and aberrant activation of growth-regulating signals such as receptor tyrosine kinases, PI3K/AKT, and mammalian target of rapamycin (mTOR) pathway [15–19]. mTOR plays a crucial role in the regulation of protein synthesis, proliferation, cell cycle progression, and survival [20]. It is essential for cell growth and G_1/S transition in cancer cells [21], by inducing translation and stability of Cyclin D1 [22]. The mTOR activation supports survival under therapeutic stress, which may lead to a drug-resistant phenotype [15, 23]. Additionally, epigenetic alterations may influence drug resistance, and many clinical studies endorse co-treatment with conventional chemotherapy and epigenetic modifier drugs [24–26].

Targeting mixed lineage leukemia (MLL or KMT2A) histone methyltransferase has been explored in drug-resistant cancers, including CRPC, leukemia, and triple-negative breast cancer (TNBC) [27–30]. Menin, the N-terminal MLL partner, is of particular interest due to its role in key oncogenic pathways involving MLL, Lens epithelium-derived growth factor (LEDGF), Enhancer of zeste homolog 2 (EZH2), and MYC [30–35]. While several studies have shown the importance of silencing in PC or CRPC [29, 36, 37], the role of Menin in taxane resistance in CRPC has not been fully understood. Since Menin inhibitors are mainly being tested in clinical trials for hematological malignancies, non-small cell lung cancer, pancreatic, and colorectal cancer [38, 39], understanding Menin's role in drug resistance could quickly adapt its consideration to overcome taxane resistance in CRPC patients.

Previously, we generated the taxane-resistant CRPC models and explored their epigenetic vulnerabilities [6]. Herein, we identified MLL-Menin and MLL-WD Repeat Domain 5 (MLL-WDR5) inhibitors as promising epigenetic therapies to overcome drug resistance. Targeting Menin selectively inhibited the growth of resistant cells, while Menin depletion in parental cells prevented the development of drug resistance, emphasizing its critical role in resistance acquisition. Notably, Menin knockout caused negative enrichment of mTOR signaling and E2F target gene sets in resistant cells. Furthermore, co-treatment with docetaxel and the mTOR inhibitor (Torin-1) improved the taxane response in Menin-depleted resistant cells. CUT&RUN-sequencing and ChIP-qPCR analyses confirmed that Menin binds to the promoters of mTOR, Cyclin D1, and CDK20, highlighting its role in sustaining taxane resistance and regulating cell cycle progression. This regulatory activity led to reduced cellular proliferation and induced G_1 cell cycle arrest in Menin-depleted, taxane-resistant cells. Ultimately, Menin knockout completely abolished tumor formation in our in vivo docetaxel-resistant CRPC model, underscoring its potential as a therapeutic target.

Materials and methods

Generation of resistant cells

The Du145 and 22Rv1 cells (ATCC, #HTB-81; ATCC, #CRL-2505) were grown in RPMI-1640 media (Gibco, #11875093) supplemented with 10% FBS (Biowest, S1810) and 1% streptomycin/penicillin (Biowest, #L0022) in a 37 °C incubator with 5% CO_2. Du145 and 22Rv1 cells were exposed to Docetaxel (Sigma #01885) for 72 h with the IC_{50} dose (1 nM, initially) to establish drug resistance. The remaining population was allowed to recover in a drug-free medium. Subsequently, drug-recovered cells were subjected to a doubled dose of Docetaxel, and this cycle continued until cells reached a more than 100-fold increase in IC_{50}. Docetaxel was prepared as a 500 mM main stock in DMSO (Sigma, #D2650). Throughout the manuscript, drug-sensitive parental cells are referred to as "P", whereas docetaxel-resistant cells are designated "DtxR".

Sulforhodamine B (SRB) viability assay

P or DtxR cells (4×10^3 cells for Du145, and 8×10^3 cells for 22Rv1) were seeded on 96-well plates 16 h before drug treatment. At the end of the exposure period, the cells were fixed with 10% (w/v) TCA (Sigma, #T6399) at 4 °C for 1 h, then TCA was washed off with dH_2O, and the plates were dried. The wells were stained with 50 µl of 0.4% (w/v) SRB (Santa Cruz, #sc-253615) for 30 min, followed by washing with 1% acetic acid and drying the plates. The SRB dye was dissolved using 150 µl of 10 mM Trizma base (Sigma, #T1503), and measurements were performed at 564 nm using a microplate reader (Synergy H1 Hybrid reader, BioTek). MI-2 (Cayman Chemical, #29218), MI-3 (Cayman Chemical, #27214), MI-136 (Cayman Chemical, #19245), MI-463 (Cayman Chemical, #33525), WDR5-0103 (Cayman Chemical, #13945), Palbociclib (Cayman Chemical, #16273), Abemaciclib (Cayman Chemical, #17740), CINK4 (Cayman Chemical, #17974), Ribociclib (Cayman Chemical, #17666),

Ryuvidine (Cayman Chemical, #16614), MHY1485 (Cayman Chemical, #18008), Epigenetics Screening Library (Cayman Chemical, #11076) were used for cell viability assays.

Colony formation assay

P or DtxR cells (1×10^3 cells for Du145, and 2×10^3 cells for 22Rv1) were seeded on 12-well plates 16 h before drug treatment. After treatment for 72 h, cells were cultured in a drug-free medium for 10–12 days. Colonies were fixed with methanol (Merck, #1.06009) for 10 min at -20 °C, stained with 0.5% (w/v) crystal violet (Merck, #1.09218) for 20 min, and then the dye was washed twice with distilled water. The quantification of colonies was performed using CellCounter software by Nghia Ho.

Cell cycle analysis

Cells were fixed with 70% ethanol (Merck, #100983) at -20 °C for at least 3 h. Residual ethanol was removed with PBS wash, and the cell pellet was stained with 200 µl of Cell Cycle Reagent (Luex Corporation, #MCH100106) for 20 min at RT in the dark. DNA content was analyzed by using the Muse Cell Analyzer, counting 5000 events.

Caspase-3/7 assay for apoptosis analysis

DtxR (1×10^5 cells/well) cells were seeded on 6-well plates 16 h before drug treatment. Muse™ caspase-3/7 reagent (CYTEK BIO, SKU #MCH100108) was diluted in PBS with a ratio of 1:8 and mixed with cell suspension. The mixture was incubated for 30 min in a 37 °C incubator with 5% CO_2. Muse™ Caspase 7-AAD working solution was added (Muse™ Caspase 7-AAD was diluted in 1 × Assay Buffer with a ratio of 1:75), and the tubes were incubated at RT for 5 min in the dark. Cells were counted by using the Muse Cell Analyzer, counting 5000 events.

siRNA-mediated silencing

siControl (Thermo Fisher Scientific, #4390843), siMLL (Ambion, #AM107890), siMEN1 (Ambion, #AM143227), and siWDR5 (Ambion, #AM136959) were used for silencing experiments. P and DtxR (2 × 10 5 cells/well) cells were seeded on 6-well plates 16 h before transfection. 75–100 pmol of each siRNA was transfected into the cells using Lipofectamine (Invitrogen, #L3000001) following the manufacturer's protocols.

RT-qPCR

RNA samples were extracted using the Quick-RNA™ Microprep Kit (Zymo Research, #R1050) and reverse transcribed into cDNA with M-MLV Reverse Transcriptase (Thermo Fisher Scientific, #28025013). RT-qPCR amplification was performed with 10 ng of cDNA and 150 nM of gene-specific primers (listed in Table S1) using LightCycler 480 SYBR Green I Master mix (Roche Diagnostics, #04707516001). The experiment was run on a LightCycler 480 (Roche Diagnostics) and incubated at 95 °C for 5 min, followed by 40 cycles of 95 °C for 10 s, 58 °C for 30 s, and 72 °C for 30 s. The relative amounts of gene expression were calculated with the $2^{(-\Delta\Delta CT)}$ method.

Protein extraction and western blotting (WB)

Cells were lysed in RIPA Lysis Buffer (Sigma Aldrich, #R0278) containing 1 × Protease Inhibitor Cocktail (Cell Signaling Technology, #5871) on ice for 15 min. The suspension was centrifuged at 17000 g for 20 min at 4 °C. Concentration analysis was performed with the Pierce™ BCA Protein Assay Kit (Thermo Scientific™, #23225). Samples (15–20 µg of whole protein) were loaded on a 4–15% SDS-PAGE gel (Bio-Rad, #161–0317). Electrophoresis was performed at 90 V for 75 min. The separated proteins were transferred onto a PVDF membrane (Bio-Rad, #1620177) at 200 mA for 120 min and immunoblotted with primary antibodies (Table S2) overnight at 4 °C. The following day, the membrane was incubated with HRP-conjugated secondary antibodies (1:5000 dilution for #ab205718, 1:5000 dilution for #ab205719) for 1 h at RT. The signal was developed by using Immobilon Forte Western HRP substrate (Millipore, #WBLUF0100) and detected with the BIORAD Chemi-Doc XRS + System. Band intensities were quantified using ImageJ software.

Analysis of clinical data

Menin mRNA levels in normal and tumor samples of Prostate Adenocarcinoma (TCGA-PRAD) were obtained from the Wanderer database using the Illumina HiSeq RNA sequencing data type [40]. Menin expression in PRAD with different Gleason scores was obtained from the TCGA Firehose Legacy study through cBioPortal [41]. Menin and mTOR mRNA expression correlation in metastatic prostate cancer was obtained from the Metastatic Prostate Cancer (SU2C/PCF Dream Team, Cell 2015) through cBioPortal [42]. Menin and Ki-67 correlation was obtained from the PRAD (TCGA, GDC) study. Clinical data showing the mTOR expression panel in patients with TNBC cancer receiving docetaxel therapy was obtained from the CTR-DBv2 database [43, 44].

Generating MEN1 and LEDGF knockout cells

The gRNA sequences were designed using Benchling software [45] as listed in Table S1. gRNA oligos were phosphorylated with T4 PNK (New England Biolabs, #M0201S) and annealed via the Feng Zheng protocol [46]. Briefly, the LentiCRISPR v2 plasmid (Addgene, 52961) was digested with BsmBI-v2 (NEB, R0739), dephosphorylated with Antarctic Phosphatase (NEB,

#M0289), and purified using the NucleoSpin Gel and PCR Cleanup kit (Macherey-Nagel, #740609). Phosphorylated gRNA oligos and LentiCRISPR v2 plasmid were ligated with T4 DNA ligase (NEB, #M0202S). Transformation was performed with stbl3-competent bacteria with a heat shock protocol, and plasmids were isolated with the Macherey-Nagel MidiPlus Plasmid Isolation Kit (#740410). HEK293T (ATCC, CRL-11268) cells were co-transfected with psPAX2 (Addgene, #12260), pVSVg (Addgene, #14888), and guide-cloned lentiCRISPRv2 plasmids with PEI (ABP Bioscience, #P017-1) according to the manufacturer's protocol. Lentiviral particles were collected and filtered (0.45 µm) on the 2nd and 3rd days of the transfection. Protamine sulfate (8 µg/ml, Thermo Fisher Scientific, #A11559II) was used to improve transduction efficiency; 2–10 µg/ml of puromycin (Thermo Fisher Scientific, #J61278.MB) was used for selection, and knockout efficiency was confirmed via western blotting using anti-MEN1 antibody (Table S2).

Generation of the MEN1-rescue system

To circumvent Cas9 activity, MEN1 cDNA was mutated. To destroy the NGG site with point silent mutation, Q5 Site-Directed Mutagenesis Kit (NEB, #E0554) protocols were followed. pBABE Hygro WT MEN1 (Addgene plasmid, #11024) was used, and the obtained plasmid carrying PAM mutation was generated. Primer sequences are provided in Table S1. To improve viral transduction efficiency, WT-MEN1 sequences were cloned into a lentiviral overexpression plasmid (Addgene, #163447). All mutations were confirmed by whole plasmid sequencing. Transfection of HEK293T cells and virus production were performed as described in detail above.

Competition assay

Menin knockout-resistant cells were labeled with mCherry fluorescent protein and sorted with the Sony SH800 Cell Sorter. Equal numbers (1:1) of control and Menin knockout-resistant cells were mixed, seeded, and co-cultured for 10 days. At the end of the co-culturing period, the percentage of mCherry signal in the mixed population was measured by Beckman Coulter Cytoflex flow cytometry.

RNA-seq and gene set enrichment analysis (GSEA)

RNA-seq analysis was performed as formerly described by [6], and GSEA was performed using GSEA_4.3.2.app. Preranked DEG file.rnk (FDR ≤ 0.05) was uploaded, and the comparison was performed with h.all.v2023.1.Hs.symbols.gmt, c5.go.bp.v2023.2.Hs.symbols.gmt, c5.go.cc.v2023.2.Hs.symbols.gmt, c5.go.mf.v2023.2.Hs.symbols.gmt, c6.all.v2023.2.Hs.symbols.gmt datasets in the MsigDB database. Enrichment bubbles were generated by using the SRplot software [47].

Generation of flag-tagged MEN1 overexpression system

MEN1 cDNA sequence was amplified using Du145 cDNA pool with the forward and reverse primers covering the beginning and end of the cDNA sequences with NheI and NotI cut site additions, respectively. Stop codon was excluded for 3×FLAG addition. A PCR reaction was performed with NEB Phusion High Fidelity DNA polymerase, using 100 ng cDNA and 125 nM of each primer. PCR reaction incubated at 98 °C for 30 s, followed by 40 cycles of 98 °C for 10 s, 72 °C for 30 s, and 72 °C for 120 s. PCR products were run on agarose gel electrophoresis for base pair validation. PCR products were cleaned with Macherey-Nagel Gel and PCR clean-up kit (#740609). The pLJC2-GPT2-3×FLAG (Addgene, #163447) plasmid was cut with NheI (NEB, #R3131) and NotI (NEB, #R3189) enzymes, and the backbone was dephosphorylated with Antarctic Phosphatase (NEB, #M0289) and purified. The PCR product with compatible ends and the lentiviral backbone was ligated with T4 DNA ligase (NEB, #M0202). The transformation was performed with stbl3-competent bacteria with a heat shock protocol, and plasmids were isolated with the Macherey-Nagel MidiPlus Plasmid Isolation Kit (#740410). HEK293T cells were co-transfected with psPAX2 (Addgene, #12260), pVSVg (Addgene, #14888), and EV-3×FLAG or MEN1-3×FLAG plasmids using PEI (ABP Bioscience, #P017-1) according to the manufacturer's protocol. Lentiviral particles were collected, filtered, and transduced into cells with Protamine sulfate (8 µg/ml). Selection was performed with 2–10 µg/ml of puromycin, and validation of the overexpression was confirmed via western blotting using FLAG and MEN1 antibodies (antibodies are listed in Table S2).

Constitutive silencing via ShRNA

HEK293T cells were co-transfected with pUMVC (Addgene, #8449), pVSVg (Addgene, #14888), and MEN1sh-pLKO1 plasmid carrying puromycin resistance with PEI (ABP Bioscience, #P017-1) according to the manufacturer's protocol. shFF (firefly luciferase) or shMEN1 carrying retroviral particles were collected, filtered, and transduced into the cells with Protamine sulfate (8 µg/ml). 2 µg/ml of puromycin was used for selection, and validation of silencing was confirmed via western blotting using MEN1 antibody (Table S2).

CUT&RUN assay and data analysis

CUT&RUN was performed according to the manufacturer's protocol. Briefly, 2×10^5 cells were bound to Concanavalin A magnetic beads for each condition. Digitonin was used to permeabilize the cell membrane, allowing primary antibodies and the pAG-MNase fusion enzyme to access the nuclei. Antibody treatment was applied to the permeabilized, bead-bound cells using 5 µg of FLAG antibody (Sigma-Aldrich, #F3165) and 5 µg of a

non-specific IgG control antibody (Thermo Fisher Scientific, #10400 C). The samples were incubated overnight at 4 °C. The following day, the pAG-MNase enzyme was added, and DNA cleavage was initiated by adding 3 µl of cold Ca^{2+}, followed by incubation at 4 °C for 30 min. To release DNA fragments, samples were incubated at 37 °C for 10 min. DNA was then purified using spin columns, following the protocol of the CST DNA Purification Kit (#14209). Sequencing libraries were prepared using the NEBNext® Ultra™ II DNA Library Prep Kit for Illumina® (NEB #E7645S/L) and sequenced on the Illumina HiSeq 3000 platform. Raw FASTQ files were processed using the nf-core CUT&RUN pipeline (v3.2.2). Adapter sequences and low-quality bases were trimmed with Trim Galore (v0.6.6), and quality was assessed using FastQC (v0.12.1). Clean reads were aligned to the hg38 reference genome using Bowtie2 (v2.4.4). PCR duplicates were removed using Picard or SAMtools to reduce bias in downstream analyses. Peak calling was performed with SEACR (v1.3), and consensus peaks were merged using bedtools (v2.31.0). Genomic tracks were visualized using IGV (v2.16.1). Final outputs—including peak statistics, fragment size distribution, and signal tracks—were summarized and visualized using deepTools. Peak annotation was carried out using HOMER's annotatePeaks.pl script.

ChIP-qPCR

EV-3×FLAG and MEN1-3×FLAG overexpressing resistant cells (3×10^6 cells/pulldown) were crosslinked, sheared, and pulled down as described in our previous report [6]. Briefly, 5 µg of FLAG antibody (Sigma Aldrich, #F3165) and a non-specific IgG antibody (Thermo Fischer Scientific, #10400 C) were mixed with Dynabeads® (Thermo Fisher protein A magnetic beads, #10001D). Next, the antibody-bead complex was incubated with pre-cleared chromatin overnight at 4 °C with rotation. The magnetic beads were washed with ChIP lysis buffer, low-salt buffer, high salt buffer, LiCl-containing buffer, and Tris-EDTA solution twice for 5 min, respectively. ChIP'ed DNA was eluted using an elution buffer containing 1% SDS (Bio-Rad, #1610418) and $NaHCO_3$ (0.1 M, Merck, #S6014) for 30 min at RT with rotation. The eluted DNA-protein complex was reverse crosslinked and purified by using the ChIP DNA Clean & Concentrator kit (Zymo Research, #D5205). Promoter regions for target genes were obtained from the Eukaryotic Promoter DataBase (EPD) [48]. Primers were designed using the NCBI primer designing tool [49], and primer sequences are listed in Table S1. For the quantitative and simultaneous analysis of immunoprecipitated DNA, qPCR was run on the LightCycler 480 (Roche). ChIP-qPCR results were calculated by the % input method.

Generation of CRPC in vivo model

Twelve SCID mice (6–8 weeks old) were housed under appropriate conditions at the Koç University Animal Facility. All experimental procedures were approved by the Koç University Institutional Ethics Board (Protocol No: 2022.HADYEK.030). Stable Du145-P and Du145-DtxR cell lines expressing Firefly Luciferase (Fluc) and mCherry were generated via viral transduction. For tumor implantation, six mice were used per group. Du145-P (1×10^6 cells) and Du145-DtxR (6×10^6 cells) were injected subcutaneously into each mouse in 100 µl of 1:2 diluted Matrigel (Cultrex, 3432-005-01). Tumor growth was monitored weekly using an IVIS Lumina III Bioluminescence Imaging System. Fluc activity was assessed by intraperitoneal injection of D-Luciferin (GoldBio, 115144-35-9) at a dose of 150 µg/g body weight. Mice were sacrificed four weeks post-injection for downstream analyses.

Statistical analysis

Data were analyzed in Prism 10 (GraphPad Software, Inc.), and statistical tests were conducted as described in the figure legends.

Results

Targeting MLL-Menin restores taxane susceptibility in resistant CRPC

We generated docetaxel-resistant Du145 and 22Rv1 cells as previously described [6]. Briefly, cells were treated with taxane for 72 h, and the surviving fractions were allowed to grow until they completely recovered (Fig. 1A). This dose increment strategy was implemented until the cells achieved more than a 100-fold increase in their IC_{50} value. Drug-sensitive parental cells ('P') and docetaxel-resistant cells ('DtxR') were used throughout the study, and the resistance profile was evidenced through cell viability assays. In both cell line models, even at elevated doses, the resistant cells retained significantly higher viability compared to their drug-naive counterparts (Fig. 1B-C and Figure S1A-B). In our previous study, we identified five groups of epigenetic enzymes that confer vulnerability in taxane-resistant CRPC models [6]. Specifically, combining taxanes with inhibitors targeting MLL-Menin, MLL-WDR5, CBP/p300, BRPF, PRMT5, and SIRT1 restored sensitivity in docetaxel- and cabazitaxel-resistant CRPC (Du145 [6], and 22Rv1) cells (Fig. 1D). It is noteworthy that this sensitization was unique to the resistant counterparts (Figure S1C). As inhibitors of MLL complex proteins are effective revertants, the focus has initially been placed on these two inhibitors, considering the vacancy in the literature regarding these inhibitors and resistance mechanisms.

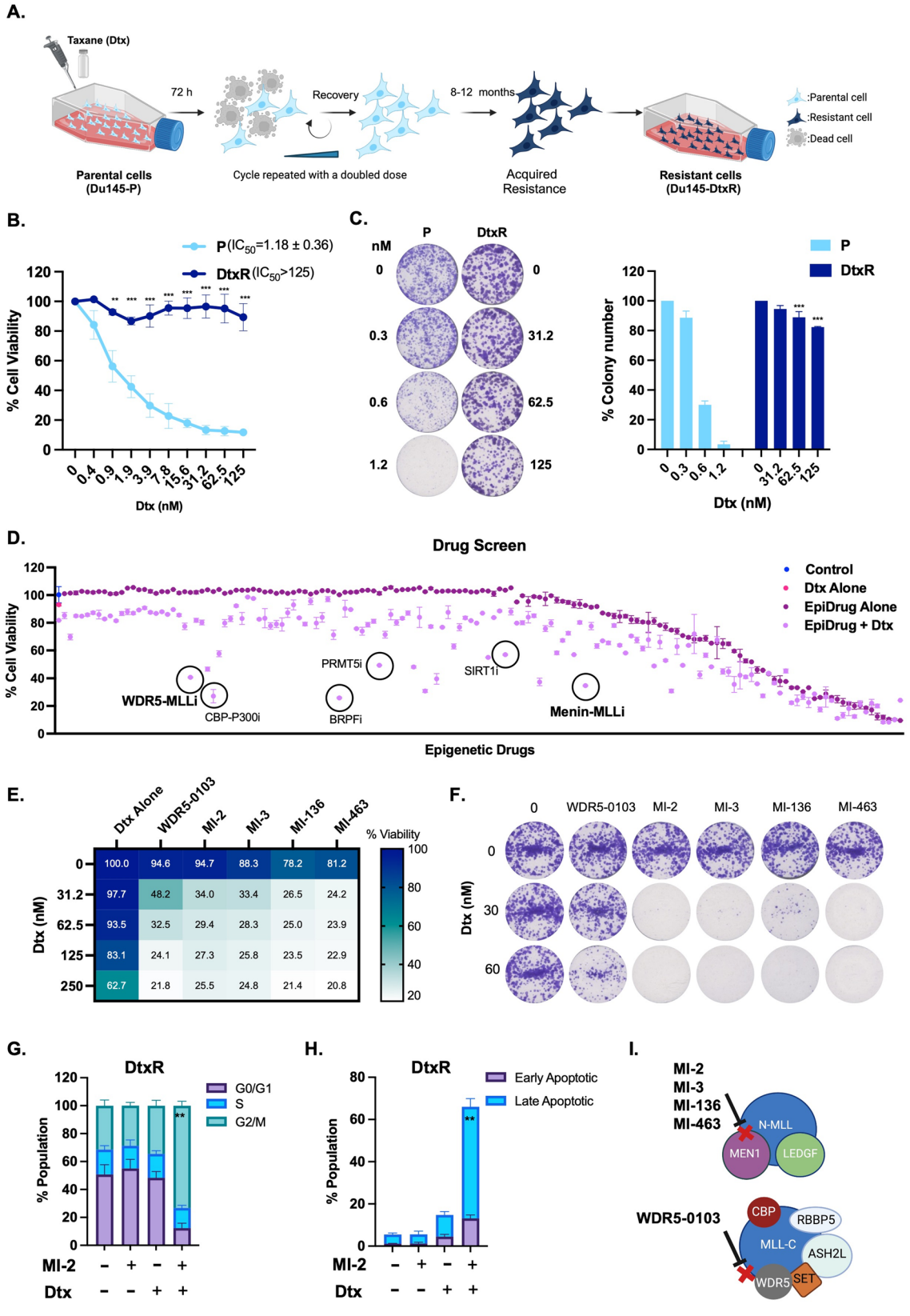


Fig. 1 (See legend on next page.)

(See figure on previous page.)

Fig. 1 Overcoming taxane resistance via targeting MLL-Menin. **A** A schematic view of the generation of docetaxel-resistant Du145 cells (Du145-DtxR). The figure was generated with BioRender. **B** Docetaxel response in both parental and docetaxel-resistant cells. Cell viability was evaluated using the SRB assay after 72 h of taxane treatment. **C** The left panel displays the colony formation analysis of parental and resistant cells following the indicated docetaxel treatments. The right panel shows the normalized colony numbers of parental and resistant cells. Colonies were quantified via Cell Counter software by Nghia Ho. **D** An epigenetic drug library was used for screening, where docetaxel-resistant cells were co-treated with 250 nM of docetaxel and 5 µM of the epidrugs for 72 h. Cell viability was assessed using the SRB assay. The following epi-drugs were validated for their ability to reverse taxane resistance: MI-2 (Menin-MLL inhibitor) and WDR5-0103 (WDR5-MLL inhibitor). Data represent the average of ± standard error of the mean. Cell viabilities for different MLL-Menin and MLL-WDR5 inhibitors, combined with increasing doses of docetaxel, were evaluated using (**E**) SRB and (**F**) colony formation assays. **G** Cell cycle distribution in Du145-DtxR cells following treatment with a combination of MLL-Menin inhibitor (MI-2) and docetaxel. **H** Flow cytometry analysis of Caspase 3/7 activation in Du145-DtxR cells following treatment with a combination of MLL-Menin inhibitor (MI-2) and docetaxel. **I** Cartoon showing the targets of MLL-Menin or MLL-WDR5 inhibitors, created with BioRender. Data represent the average ± standard deviation of three biological repeats (t-test, $*p < 0.05$, $**p < 0.01$, $***p < 0.001$)

Based on results from the chemical screen, in both cell lines, we tested and validated the efficacy of various inhibitors of MLL-Menin (MI-2, MI-3, MI-136, and MI-463) and MLL-WDR5 (WDR5-0103) with docetaxel (Fig. 1E-F and Figure S1D-E). Interestingly, MLL inhibitors synergistically reversed the resistance when combined with taxanes in both cell models (Figure S2). G_2/M arrest is a significant indicator of taxane efficacy through inhibition of microtubule depolymerization [50]. Due to the resistance profile, docetaxel treatment was insufficient to induce an arrest in resistant cells. However, co-administration of an MLL-Menin inhibitor and docetaxel restored G_2/M arrest, further supporting the re-sensitization (Fig. 1G). This prolonged G_2/M arrest in combination treatments ultimately led to cell death through apoptosis, as evidenced by the Caspase 3/7 activation (Fig. 1H). MI-2, MI-3, MI-136, and MI-463 disrupt the MLL–Menin interaction, whereas WDR5-0103 inhibits the catalytic activity of MLL and WDR5 (Fig. 1I). Since these compounds target three distinct components of the MLL complex, we aimed to investigate the roles of these three proteins in docetaxel resistance.

siRNA knockdown of MLL, Menin, and WDR5 demonstrated that MLL and WDR5 are essential for the survival of both parental and resistant cells, consistent with their broad roles in epigenetic regulation and oncogenic transcription [51, 52]. In contrast, Menin silencing selectively impaired the proliferation of resistant cells (Fig. 2A). We subsequently assessed Menin mRNA levels between prostate adenocarcinoma samples and normal prostate tissues using publicly available RNA-seq data (TCGA-PRAD) obtained by the TCGA Wanderer database. Notably, Menin mRNA was significantly upregulated in tumor samples compared to normal tissues (Fig. 2B), which directed our interest toward investigating Menin dependency in resistant cells. While few studies have highlighted the role of Menin and MLL complexes in androgen-dependent PC [29, 36, 37], their significance in docetaxel-resistant CRPC has remained largely unexamined, making this study the first to address this gap.

Depletion of Menin specifically reduces taxane-resistant Du145 growth

Next, we assessed the Menin expression in a TCGA data set comprising 501 samples (Firehose Legacy) from patients who underwent radical prostatectomy (GDAC-PRAD-20160128). The analysis revealed that Menin expression was elevated in samples with higher Gleason scores (Fig. 2C), which prompted us to generate Menin knockout cells and examine its impact on both parental and resistant cells. We isolated two individual knockout clones from the parental and the resistant cells (Fig. 2D). The absence of Menin in parental cells had almost no effect on cell growth, similar to what was observed with siRNA. However, in resistant cells, Menin knockout led to a significant reduction in cell growth, with KO#1 showing the most substantial decrease (Fig. 2E). The growth pace of resistant KO#1 was notably slow, which made experimental time management challenging. Therefore, in further experiments, we proceeded with KO#2, which showed a complete knockout of Menin and yielded a more manageable population size for phenotypic assessments (Fig. 2E-F). To evaluate whether the observed phenotype was Menin-specific, we performed a rescue experiment. Wild-type Menin cDNA, with a guide-specific PAM mutant, was generated to circumvent Cas9 activity. This Menin sequence was cloned into a lentiviral overexpression plasmid and introduced into the Menin-depleted cells (Fig. 2G). As demonstrated in Fig. 2H-I, wild-type Menin overexpression restored the colony numbers in Menin knockout-resistant cells.

Additionally, we generated Menin knockout models in our AR-positive PC cell line (LNCaP) and a second docetaxel-resistant CRPC cell line (22Rv1-DtxR) (Figure S3). As previously reported, targeting Menin in AR-positive PC has been demonstrated to be an effective strategy, due to direct interaction with Menin and AR [29]. Notably, our findings in LNCaP cells supported this reduction in cell growth (Figure S3A-B). Additionally, Menin depletion reduced cell growth in both parental and resistant 22Rv1 cells (Figure S3C-D). The divergent

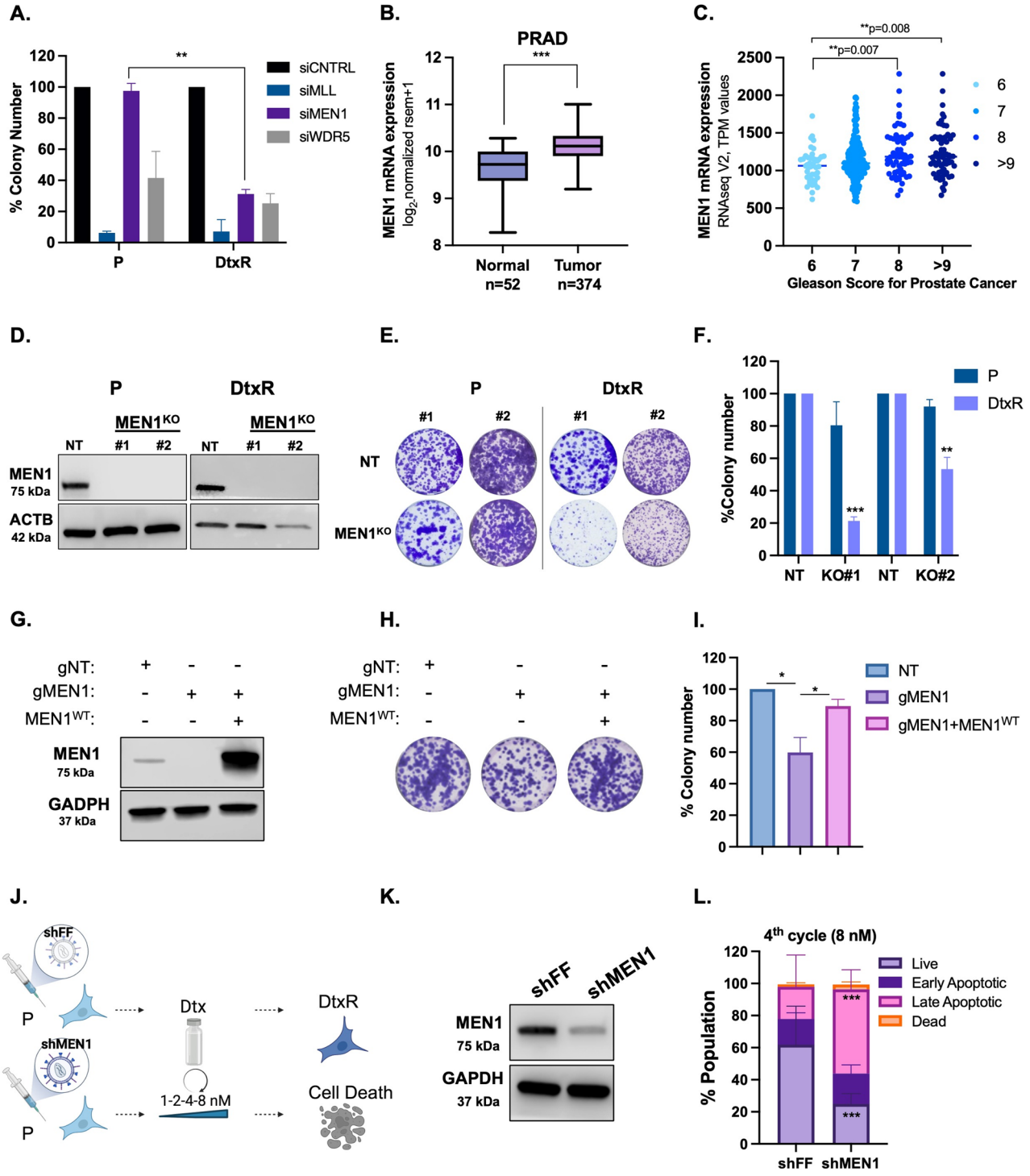


Fig. 2 (See legend on next page.)

(See figure on previous page.)

Fig. 2 Menin is critical for sustaining docetaxel-resistant CRPC and enabling resistance development in parental cells. **A** Parental and resistant Du145 cells were treated with siControl, siMLL, siMEN, and siWDR5, and the graph shows the normalized colony numbers. Data represent the average ± standard deviation of three biological repeats (t-test, $^{**}p < 0.01$). **B** Clinical data representing mRNA levels of prostate adenocarcinoma patients were obtained from the TCGA-PRAD dataset accessed through the TCGA Wanderer database. The x-axis represents normal and tumor samples, while the y-axis represents normalized RNA-seq V2 values (log_2_normalized rsem + 1). **C** Scatter plots of Menin mRNA levels in clinical samples (TCGA, Prostate Adenocarcinoma-Firehose Legacy) were assessed by using the cBioPortal; the x-axis represents Gleason scores of the specimens, while the y-axis represents RNAseq V2 values (normalized transcript per million, TPM values) by *RSEM*. **D** Western blot showing depleted Menin levels in two individual knockout clones generated by CRISPR in parental and resistant Du145 cells. **E** Colony-forming ability of Menin knockout clones in parental and resistant cells. **F** Normalized colony numbers in Menin knockout cells. **G** Western blots showing depleted and restored Menin protein levels in Du145-DtxR cells. **H** The corresponding colony-forming ability of Menin-depleted and rescued Du145-DtxR cells. **I** Normalized colony numbers in Menin knockouts, restored by wild-type Menin. **J** Illustration of re-establishing docetaxel resistance in Menin-silenced parental cells. The figure was generated with BioRender. **K** Validation of protein knockdown efficiency in shMEN1-treated parental Du145 cells via western blot analysis. **L** The distribution of apoptotic populations in Menin-expressing and Menin-depleted parental Du145 cells during the development of resistance to docetaxel was analyzed using Annexin-V staining following treatment with 8 nM docetaxel

responses to Menin loss between the two parental CPRC models may be explained by their differential AR expression. Although both cell lines represent CRPC, 22Rv1 cells express AR, whereas Du145 cells lack AR expression [53]. However, which advantages Menin conferred to docetaxel-resistance, particularly in AR-absent models such as Du145, still intrigued us.

Menin is indispensable for the acquisition of drug resistance in CRPC

To assess the role of Menin in the acquisition of drug resistance, we silenced Menin constitutively in parental cells and attempted to re-establish resistance by exposing these cells to docetaxel (Fig. 2J-K). Following the fourth treatment cycle, control cells (shFF) survived the docetaxel treatment, and this remaining population exhibited a drug-resistant phenotype. In contrast, approximately 80% of the Menin-silenced parental cells underwent apoptosis, suggesting that Menin is essential for the cells' acquisition of drug resistance, as the remaining population was unable to recover and failed to adapt to the process (Fig. 2L).

Transcriptomic analysis reveals key biological processes contributing to drug resistance

These cumulative findings prompted us to focus on the N-terminal MLL target Menin to uncover the mechanisms contributing to taxane resistance. To reveal Menin-dependent transcriptional differences between parental and resistant cells, we performed RNA sequencing comparing (i) parental versus resistant cells, and (ii) wild-type versus Menin-null conditions in both parental and resistant settings. The transcriptomic differences between our parental and resistant cells, as well as the ABCB1-mediated drug resistance mechanism through BRPF1, have been reported previously [6]. To assess whether Menin's role in resistance might involve ABCB1, we first examined their interaction using Menin inhibitor or Menin knockout models; however, no significant regulation was observed. Additionally, Menin did not show significant enrichment on the ABCB1 promoter in our resistant cell model (Figure S4), supporting the conclusion that Menin-mediated resistance occurs through alternative pathways. We then specifically analyzed RNA-seq data from Menin wild-type and two different Menin null clones in resistant cells (NT, KO#1, and KO#2). As illustrated in the PCA plot (Fig. 3A), each clone clustered closely with its biological replicate, and Menin loss resulted in similar transcriptomic alterations across both clones. The *d*ifferentially *e*xpressed *g*enes (DEGs) those were commonly altered in both clones ($MEN^{KO\#1} \cap MEN^{KO\#2}$) in the same direction (upregulation or downregulation) relative to gNT were overlapped, and genes meeting the criteria FDR < 0.05 and $|Log_2FC| \geq 0.5$ were considered statistically significant. In common DEGs between two Menin knockouts, 2077 genes were upregulated, and 2120 genes were downregulated upon Menin knockout, as depicted in Fig. 3B.

Given that Menin ablation significantly impeded the growth of resistant colonies, we focused on the potential advantages Menin may confer to resistant cells. To this end, we compared the genes showing opposite directions in DtxR and following Menin knockout. Among these, 798 (330 up to down and 468 down to up) genes reversed direction in response to Menin ablation (Figure S5A). Interestingly, as cells transition from a drug-naive state to a resistant phenotype, gene sets related to E2F targets, G_2M checkpoint, and mTOR signaling showed positive enrichment (NES values of 2.78, 2.09, and 1.78, respectively) (Figure S5B) [6]. In contrast, these gene sets exhibited a complete reversal in the absence of Menin, with NES values of (-1.46), (-1.32), and (-1.04), respectively (Fig. 3C-D). Menin ablation led to negative enrichment of gene sets, including the MLL complex and histone lysine methylation, providing additional validation of our knockout models (Fig. 3C).

Menin regulates mTOR expression and its depletion, along with mTOR inhibition, further sensitizes the cells to docetaxel

To investigate how Menin supports the transcriptional programs active in resistant cells, we revisited our GSEA results. During the acquisition of resistance, mTOR

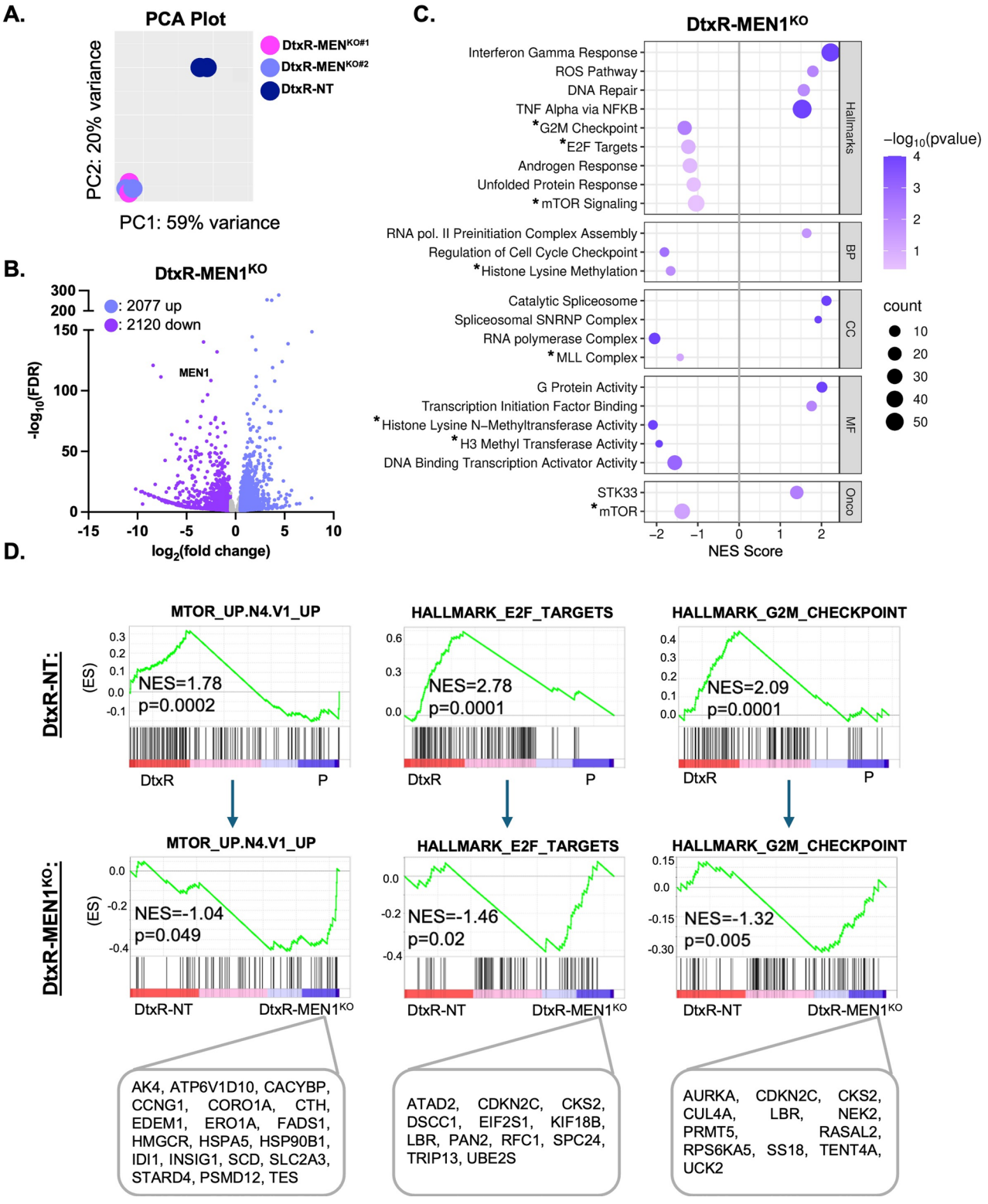


Fig. 3 Transcriptome analysis reveals differentially enriched gene sets in Menin knockout-resistant cells. **A** PCA plot showing transcriptomic differences between two different clones of Menin knockout and their controls in DtxR cells. **B** Volcano plot illustrating common DEGs between knockout clones ($MEN1^{KO\#1} \cap MEN1^{KO\#2}$) (each dot represents a gene in $MEN1^{KO\#2}$, meeting the criteria of FDR < 0.05 and $|Log_2FC| \geq 0.5$). **C** Enrichment bubble plot showing the enriched gene sets in control and $MEN1^{KO}$ DtxR cells from the GSEA (MSigDB) database in Hallmarks, Molecular Functions (MF), Biological Processes (BP), Cellular Compartments (CC), and Oncogenic Signature collections, visualized using the SRPlot. **D** The NES values for E2F targets, G_2/M checkpoint, and mTOR signaling upon DtxR cells or Menin knockout DtxR cells. Negatively enriched genes upon Menin knockout are also given under the gene sets

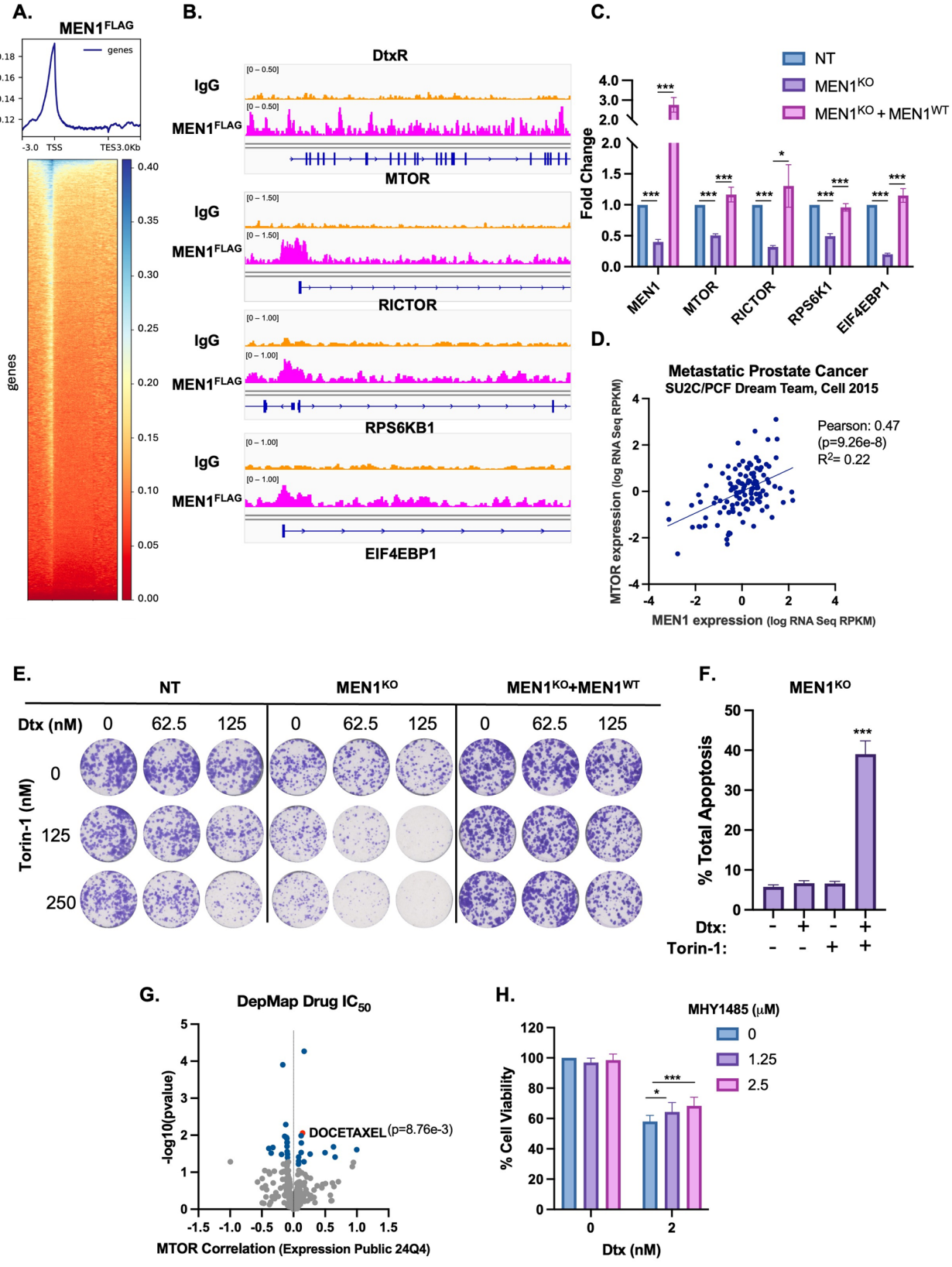


Fig. 4 (See legend on next page.)

(See figure on previous page.)

Fig. 4 Menin is enriched at the mTOR promoter, and its depletion sensitizes resistant cells to a combined treatment of the mTOR inhibitor (Torin-1) and docetaxel. **A** CUT&RUN analysis in DuDtxR cells reveals the genomic localization of Menin on the TSS region in differentially expressed genes. **B** Menin enrichment on the mTOR promoter and its downstream targets. **C** Expression levels of mTOR and its downstream targets in Menin knockout and rescued DtxR cells. **D** Correlation between MEN1 and mTOR expression levels in metastatic PC. Data sources include Metastatic Prostate Cancer (SU2C/PCF Dream Team, Cell 2015) obtained from the cBioPortal software. **E** Colony formation of Menin wild-type, knockout, and rescued DtxR cells with Torin-1 and docetaxel treatment. **F** Annexin-V and 7-AAD staining of Menin knockout cells following treatment with Torin-1 and docetaxel. Data represent the standard deviation of three biological repeats (t-test, ***$p < 0.001$).**G** The volcano plot shows the sensitivity of various cancer cell lines (IC_{50} values) to a wide range of drugs based on their mTOR expression levels. Blue dots represent drugs with significant correlations, where the left side indicates lower IC_{50} values (greater drug sensitivity), and the right side indicates higher IC_{50} values (greater drug resistance). The red dot represents the response to Docetaxel. **H** Activating the mTOR pathway via MHY1485 for 6 h in Du145 parental cells and cell viability in response to Docetaxel following mTOR activation

signaling, E2F targets, and the G_2/M checkpoint were enriched in the positive direction, reflecting coordinated activation of these pathways. Upon MEN1 knockout, these pathways shifted to negative enrichment, indicating their attenuation (Fig. 3D). The leading-edge genes associated with this negative transition are shown in Fig. 3D, providing a clearer view of the transcriptional basis underlying the pathway-level changes. Collectively, this data indicates that docetaxel-resistant cells adopt a growth-signaling–activated, checkpoint-engaged transcriptional state, characterized by activation of mTOR signaling, E2F-driven transcription, and the G_2/M checkpoint. Functional perturbation reveals that Menin is required to maintain these pathway activities. Thus, resistant cells exhibit a dependency on Menin to sustain adaptive pathway activation during taxane resistance, and targeting Menin may contribute to re-sensitization. Supporting this connection, a review of publicly available ChIP-seq datasets revealed prominent Menin binding peaks around the mTOR promoter in leukemia cell lines [54–58]. These findings prompted us to further explore the Menin-mTOR relationship in our taxane-resistant model.

We conducted CUT&RUN analysis to assess Menin's chromatin occupancy in Du145-DtxR cells. Using SEACR (v1.3), we identified 2589 chromatin peaks. Menin binding was predominantly enriched at transcription start sites (TSS) of target genes (Fig. 4A). IGV track analysis revealed significant Menin occupancy at the promoter regions of *mTOR*, *Rictor*, *RPS6KB1*, and *EIF4EBP1* genes (Fig. 4B). These findings were further validated by ChIP-qPCR, confirming Menin's enrichment at the mTOR promoter (-500 bp to + 100 bp) in Du145-DtxR cells (Figure S6A-B). We next assessed the expression of these target genes in Menin knockout and rescued cells. Gene expression levels were significantly reduced in the absence of Menin and were restored upon Menin re-expression (Fig. 4C). Lastly, analysis of patient datasets revealed a significant correlation between Menin and mTOR expression in metastatic PC, with a Pearson correlation coefficient of 0.47 (Fig. 4D).

Given that several mTOR inhibitors are in clinical trials, we asked whether they could be used on taxane-resistant cells. Indeed, simultaneous mTOR inhibition (via Torin-1) and Menin depletion further enhanced the taxane response (Fig. 4E, Figure S5C). This phenotype was reversed upon the restoration of Menin expression, showing that Menin is involved in regulating mTOR expression and determining the effectiveness of mTOR signaling inhibition. The critical role of Menin status in determining the taxane response may be linked to the decreased expression of mTOR and its related downstream signaling in the absence of Menin. In this cellular environment, the use of an inhibitor seems to affect the residual mTOR signaling essential for taxane resistance, resulting in a significantly improved taxane response compared to Menin wild-type cells. Accordingly, Menin knockout cells demonstrated increased levels of apoptosis in response to the docetaxel and Torin-1 combination (Fig. 4F). We also used the DEPMAP portal to analyze drug response in different cell lines regarding mTOR expression levels. In 328 cell lines tested, higher mTOR expression positively correlated with the increase in Docetaxel IC_{50} (Fig. 4G). Finally, activation of the mTOR pathway via MHY1485 also decreased the Docetaxel response in our parental cells (Fig. 4H). These findings underscore the functional interaction between Menin and mTOR and support the therapeutic potential of co-targeting these pathways to overcome taxane resistance in PC.

Menin is involved in cell cycle machinery and regulates cyclin D1 and CDK20 expression

The observed reduction in cell proliferation, accompanied by decreased mTOR expression and negative enrichment of cell cycle-related genes in Menin knockout cells, prompted further investigation into the underlying mechanisms.

To investigate whether Menin promotes cell growth, we analyzed its expression in clinical data from PC cases, alongside the cell growth indicator Ki-67. Interestingly, a positive correlation was observed between high Menin expression and Ki-67 levels, suggesting a potential role for Menin in driving cell proliferation (Fig. 5A). To functionally assess this, we conducted a competition assay, labeling Menin knockout-resistant cells with a mCherry

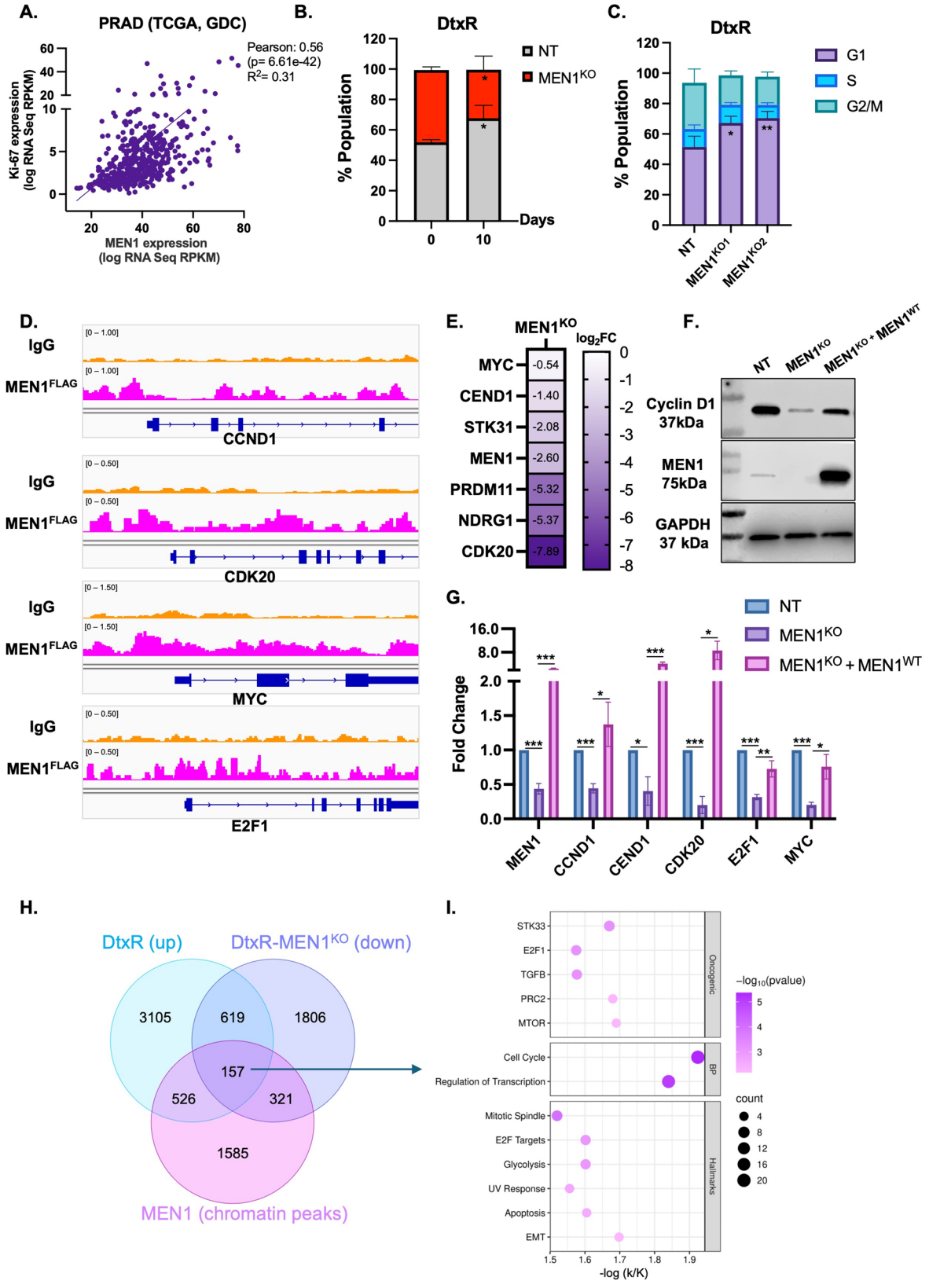


Fig. 5 (See legend on next page.)

(See figure on previous page.)

Fig. 5 Menin regulates cell cycle progression via Cyclin D1. **A** Correlation of Menin and Ki-67 proliferation marker in PRAD. The data source includes Prostate Cancer (TCGA, GDC), obtained from the cBioPortal software. **B** Population percentages of Menin wild-type and knockout cells in competition experiments over a 10-day duration. **C** Cell cycle distribution in two different Menin knockout clones. **D** Menin enrichment on the promoter of several genes in cell cycle regulation, according to the CUT&RUN analysis performed in DtxR cells. **E** Reduced expression of several genes contributing to cell cycle regulation upon Menin knockout. **F** Western blot showing Cyclin D1 protein levels in control, Menin-knockout, and Menin-rescued cells. **G** Expression levels of cell cycle regulating genes in Menin knockout and rescued DtxR cells. **H** Number of common genes upregulated in resistant cells (no FC cutoff, FDR < 0.05), downregulated upon Menin knockout (no FC cutoff, FDR < 0.05), and enriched peaks in Menin chromatin pulldown (annotated peaks in SEACR) in Du145-DtxR cells. **I** The bubble plot depicting the 157 common genes computed overlapped in the GSEA (MSigDB) database in Hallmarks, Biological Processes (BP), and Oncogenic Signature collections, visualized using the SRPlot. Bubble size represents gene number, and color indicates adjusted p-values. (k) represents the number of overlapped genes, and (K) represents the number of genes in gene sets

reporter and co-culturing them with Menin-wild-type cells for 10 days. The analysis of the mCherry signal revealed that the mixed population predominantly consisted of Menin-wild-type cells, suggesting that Menin knockout-resistant cells had a slower division rate (Fig. 5B). Consistently, cell cycle analysis showed an increased G_1 population in both Menin knockout-resistant clones (Fig. 5C). Previous studies have shown that CDK4/6 inhibitors are particularly effective against rapidly proliferating cancer cells [59, 60]. In line with their slow-cycling phenotype, Menin-knockout DtxR cells displayed reduced sensitivity to several CDK4/6 inhibitors, including Palbociclib, Abemaciclib, CINK4, and Ribociclib (Figure S7).

Next, we assessed the levels of key cyclins in non-synchronized populations of Menin wild-type and knockout clones. Cyclin D1 is essential for initiating cell division during the G_1 phase, while Cyclin E1 is predominantly expressed in late G_1 and is critical for the G_1/S transition [61]. Menin knock-out DtxR cells displayed reduced levels of Cyclin D1 and elevated levels of Cyclin E1 (Figure S8A), consistent with the G_1/S arrest phenotype.

Previous studies have shown that MEN1 enhances MYC expression, which in turn upregulates Cyclin D1 and promotes the G_1/S cell cycle progression [62, 63]. CDK20, a cyclin-dependent kinase and key regulator of the cell cycle, has been reported to activate CDK2, facilitating the G_1/S transition [64, 65] and regulating Cyclin D1 expression in tumor cells [66]. To explore whether Menin directly regulates the expression of these cell cycle-related factors, we assessed its chromatin binding profile. Our CUT&RUN-seq analysis revealed significant Menin enrichment at the promoter regions of the Cyclin D1, CDK20, MYC, and E2F1 genes (Fig. 5D). ChIP-qPCR further confirmed Menin occupancy at the promoters of these key regulators (Figure S8B). Consistently, Menin knockout cells exhibited a marked reduction in the expression of these factors (Fig. 5E), and the re-expression of Menin in knockout cells restored the expression levels of these genes (Fig. 5F-G).

Finally, a total of 157 genes were identified as commonly upregulated during resistance development, downregulated upon Menin depletion, and directly bound by Menin on chromatin (Fig. 5H). Once again, when analyzed in GSEA, computing overlaps databases, these common genes were enriched in mTOR and cell cycle gene sets (Fig. 5I). Together, these findings suggest that Menin directly contributes to the transcriptional regulation of mTOR and critical cell cycle regulators—particularly Cyclin D1 and CDK20—in taxane-resistant CRPC.

Menin loss in docetaxel-resistant CRPC led to complete suppression of tumor growth

To explore Menin's role in more clinically relevant settings, we examined the effect of Menin loss in an in vivo model. Specifically, we used xenograft models with Firefly Luciferase-mCherry-expressing Du145-P and Du145-DtxR cells, comparing control guide and Menin knockout conditions ($n = 6$) (Fig. 6A). Cells were injected subcutaneously, and tumor growth was monitored over four weeks. Parental cells successfully formed tumors, whereas tumor size was reduced in Menin-ablated cells at 3 and 4 weeks post-injection. Furthermore, Menin knockout in docetaxel-resistant cells completely abolished tumor growth compared to control cells (Fig. 6A and Figure S9-10). This loss of tumor signal likely reflects tumor-intrinsic consequences of Menin depletion, potentially driven by mechanisms such as downregulated mTOR signaling, growth arrest, apoptotic induction, or impaired vascularization. These results demonstrate an essential role for Menin in the establishment of docetaxel-resistant CRPC tumors in vivo.

We also analyzed mRNA levels in our xenograft samples and found that mTOR expression was upregulated in wild-type resistant tumors (Fig. 6B). Furthermore, IHC data from the Human Protein Atlas indicated that mTOR expression was elevated in high-grade PC tissues compared to low-grade PCs (Fig. 6C). Finally, we aimed to analyze PC patients treated with docetaxel and evaluate drug response patterns using the CTR-DBv2 database. However, suitable data for PC were unavailable. Interestingly, in the treatment response analysis of TNBC patients receiving docetaxel, a notable pattern emerged. Patients with higher mTOR pathway expression were significantly non-responsive, whereas those with lower mTOR pathway expression exhibited better responses to docetaxel treatment (Fig. 6D) [44].

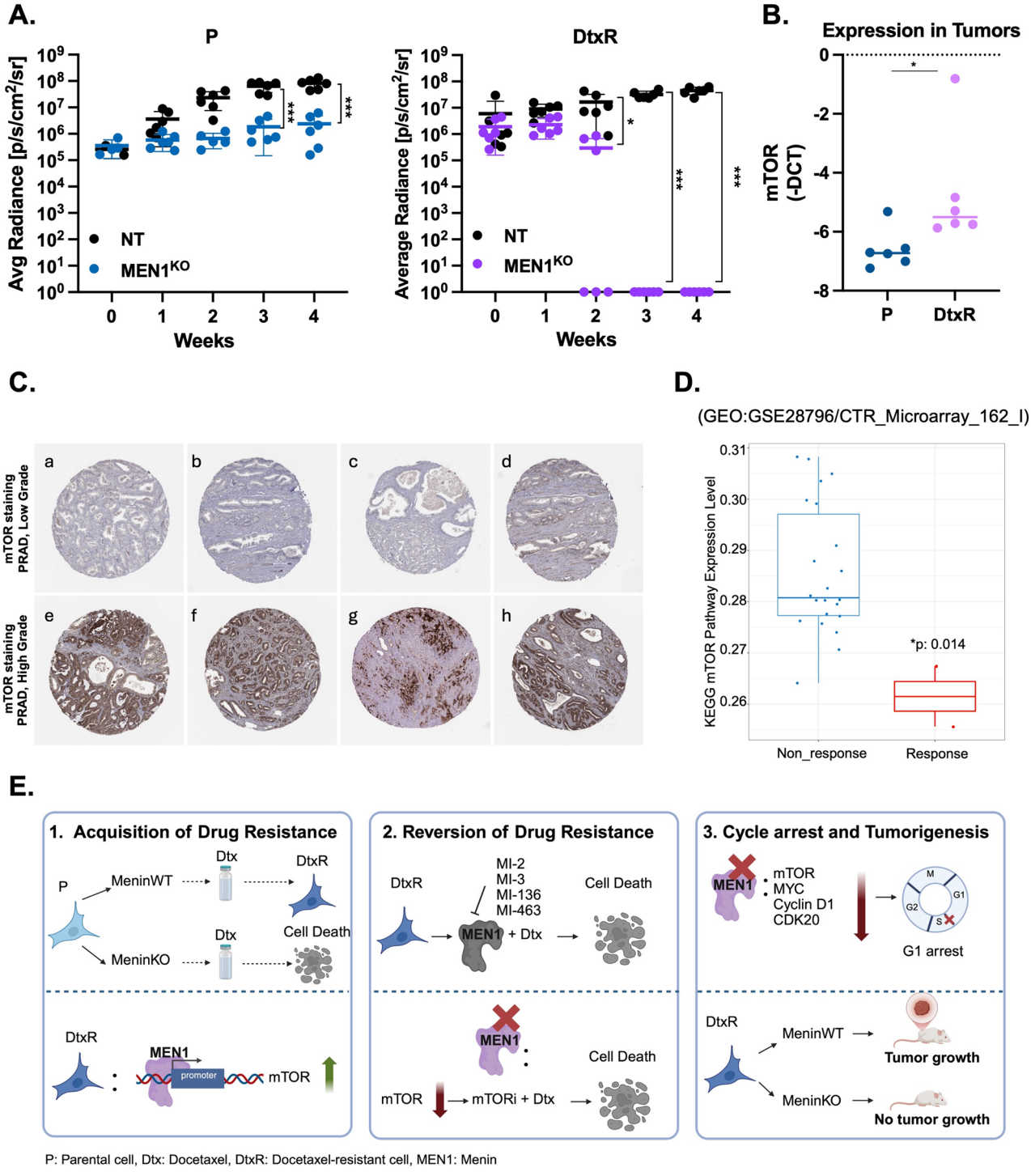


Fig. 6 Menin loss abolishes tumorigenicity in Docetaxel-resistant CRPC. **A** Relative bioluminescence signals were obtained weekly from six SCID mice injected with parental and resistant cells. Bioluminescence signal intensities were obtained using the IVIS Lumina III Bioluminescence Imager 10 min after intraperitoneal administration of D-luciferin at a dose of 150 µg/g (t-test, $*p < 0.05$, $**p < 0.01$, $***p < 0.001$). **B** Expression levels of mTOR in our xenograft models. Total RNA was extracted from tumor samples using TRIzol, and M-MLV Reverse Transcriptase was used for cDNA synthesis. Relative mRNA expression levels were quantified by qPCR using the ΔCt method and normalized to housekeeping gene expression. Each dot represents the mean value of six technical replicates from six different tumor samples. Horizontal lines indicate group means. Statistical significance was determined using an unpaired two-tailed *t*-test on mean ΔCt values. ($*p < 0.05$). **C** Immunohistochemistry images of mTOR expression in low (a-d) and high grades (e-h) of PC specimens, obtained from the Human Protein Atlas. **D** mTOR pathway expression levels in the treatment response group of TNBC patients receiving docetaxel therapy compared to the non-response group. Data was obtained from the CTR-DBv2 database. PMID: 21633166. **E** The figure summarizes the key findings of our study, highlighting Menin's regulatory role in the development and reversal of docetaxel resistance, as well as its impact on cell cycle regulation and tumorigenesis in CRPC cells. The graphical abstract was generated with BioRender

Overall, MLL-Menin inhibitors are effective in reversing taxane resistance in CRPC. Additionally, Menin contributes to taxane resistance through mTOR, making the combined targeting of Menin and mTOR a promising strategy. Furthermore, Menin depletion results in G_1 arrest and significant disruption in tumor formation in taxane-resistant CRPCs. Key findings of this study are illustrated in the graphical abstract shown in Fig. 6E.

Discussion

Drug resistance is a common phenomenon that is an obstacle to successful therapy due to several emerging mechanisms [67]. Identifying drug-specific mechanisms is crucial for uncovering potential therapeutic targets, which can lead to improved treatment outcomes. As the dynamic and reversible nature of epigenetic regulation allows for broad and impactful targeting, drug resistance research has also embraced this approach, leading to the testing of the efficacy of epigenetic inhibitors in clinical trials and FDA approval [68]. The effects of MLL targeting in both leukemia and PC have been previously demonstrated [29, 69–72]. Our group is the first to demonstrate the efficacy of MLL-Menin inhibitors in overcoming docetaxel-resistant CRPC. We found that several MLL-Menin inhibitors (MI-2, MI-3, MI-136, and MI-463) effectively re-sensitized resistant cells, yielding a significant synergy.

Menin was initially described as a tumor suppressor [73], and also exerted regulatory effects in immune cells by limiting mTORC1 activation to prevent T-cell exhaustion [74]. Later on, Menin was found to play a role in MLL-related leukemogenesis [35], and is now recognized for its oncogenic roles in various cancers, including breast, glioma, hepatocellular carcinoma, sarcoma, and PC [29, 33, 36, 37, 75–77]. Consistent with previous reports, Menin inhibition suppressed cellular growth in AR-positive PC and CRPC cell line models. In contrast, in AR-negative CRPC, it selectively impaired the growth of docetaxel-resistant cells while exerting only a minor effect on parental cells, as shown by our in vitro and in vivo studies. Menin's clinical significance was further supported by its elevated expression in tumor samples compared with normal tissues and its positive association with higher Gleason scores in PRAD. Collectively, these findings underscore the context-dependent nature of Menin–mTOR signaling, and position Menin as a promising yet cell–type–specific therapeutic target.

Menin plays a critical role in linking transcription factors to histone-modifying complexes, influencing gene expression and chromatin dynamics [78]. Menin expression was crucial for enabling drug-naive cells to acquire resistance, potentially through the upregulation of mTOR and MYC signaling, both of which are commonly associated with drug resistance and advanced tumors [23, 79–86]. Menin depletion significantly reduced these targets in our docetaxel-resistant CRPC model, and similar to our findings, Menin silencing in PC cells resulted in the downregulation of the PI3K-AKT pathway [36]. Additionally, the co-localization of Menin and MYC on chromatin emphasized their collaborative role in cancer progression [63]. Although targeting MYC directly is challenging due to the lack of druggable pockets, mTOR inhibition with temsirolimus was investigated in clinical trials for CRPC. However, the trial was discontinued due to the limited efficacy of the drug and its adverse effects, and future studies were suggested with combination approaches or novel PI3K pathway inhibitors [87]. On the other hand, Menin inhibitors have recently attracted considerable attention in clinical research, with Revumenib receiving FDA approval in November 2024 for the treatment of relapsed or refractory acute leukemias [39]. As Menin targeting and mTOR inhibition via Torin-1 exhibited significant synergy in the docetaxel-resistant CRPC model, we recommend a similar approach for future therapies.

Most cancer cells heavily rely on growth factors due to their critical role in promoting the G_1 to S phase transition, which facilitates rapid cell division [88]. Activation of receptor tyrosine kinases increases expression of Cyclin D1, the primary cyclin in the G_1 state, facilitating progression into the S phase [89]. A key phenotype observed in Menin knockout-resistant cells was their slower progression through the cell cycle, likely due to reduced mTOR and MYC activity, which may delay the rapid transition from the G_1 to the S phase. Furthermore, Menin exhibited significant enrichment of Cyclin D1 and CDK20 promoter, suggesting Menin-dependent transcriptional regulation also contributes to cell cycle progression. CDK20 and Cyclin D1 interaction was reported in promoting ovarian carcinoma growth [66]. Additionally, CDK20 depletion was shown to inhibit cancer cell proliferation [90, 91]. In line with these findings, we showed that Menin is required for maintaining Cyclin D1 and CDK20 expression, ensuring the growth of CRPC cells.

In summary, MLL-Menin inhibitors effectively reverse docetaxel resistance in CRPC. Menin acts as an essential contributor, promoting docetaxel resistance by regulating mTOR signaling. Menin also supports the growth of taxane-resistant CRPC cells, and its loss leads to G_1/S arrest. Finally, the loss of Menin eliminates tumorigenicity in docetaxel-resistant CRPC cells in xenograft models. These findings establish Menin not only as an important factor for docetaxel resistance but also as a therapeutic cornerstone, with dual targeting of Menin and mTOR offering a promising strategy to redefine treatment paradigms in taxane-refractory PC.

Supplementary Information

The online version contains supplementary material available at https://doi.org/10.1186/s12964-025-02594-1.

Supplementary Material 1.

Supplementary Material 2.

Acknowledgements

The authors gratefully acknowledge the use of the services and facilities of the Koc University Research Center for Translational Medicine (KUTTAM), funded by the Presidency of Turkey, Head of Strategy and Budget. We extend our heartfelt gratitude to Alperen Yılmaz, a former member of the Tamer Onder lab, for generating the PAM mutant in the Menin overexpression plasmid. Schematic representation figures were created in BioRender.com and licensed for publication. BioRender Publication License codes: CV27JEGI7B (Figure 1A), EL27LQD04Y (Figure 1I), RZ27JEGYA0 (Figure 2J), IC28ZPP2TY (Figure 6E).

Authors' contributions

IB conducted the in vitro experiments and wrote the paper. BC wrote and critically reviewed the paper. NY conducted the in vivo experiments. HS performed the bioinformatic analysis. TO provided genetic materials and reviewed the paper. CA conceived the project and reviewed the paper. The paper has been read and approved by all named authors.

Funding

Financial support was obtained from the Health Institutes of Türkiye (TUSEB) (Grant code: 2022-B-01-14333).

Data availability

The raw RNA-seq and CUT&RUN-seq data provided in our study have been deposited in the Gene Expression Omnibus database (accession number: GSE302154). Patient data was obtained from GEO (GSE28796) [44]. All the other data are available within the article and its Supplementary Information.

Declarations

Ethics approval and consent to participate

Koc University Local Ethics Committee approved animal experiments for Animal Experiments (HADYEK) with the protocol number 2022.HADYEK.030. No human subjects were included in the study.

Competing interests

The authors declare no competing interests.

Received: 15 July 2025 / Accepted: 4 December 2025
Published online: 18 December 2025

References

1. Sung H, et al. Global cancer statistics 2020: GLOBOCAN estimates of incidence and mortality worldwide for 36 cancers in 185 countries. CA Cancer J Clin. 2021;71(3):209–49.
2. Li G, et al. Guidelines for radiotherapy of prostate cancer (2020 edition). Precision Radiation Oncol. 2021;5(3):160–82.
3. Schroder F, et al. Androgen deprivation therapy: past, present and future. BJU Int. 2012;109:1–12.
4. Ingrosso G, et al. Current therapeutic options in metastatic castration-resistant prostate cancer. Semin Oncol. 2018;45(5–6):303–15.
5. Saad F, Miller K. Treatment options in castration-resistant prostate cancer: current therapies and emerging docetaxel-based regimens. Urol Oncol. 2014;32(2):70–9.
6. Cevatemre B, et al. Exploiting epigenetic targets to overcome taxane resistance in prostate cancer. Cell Death Dis. 2024;15(2):132.
7. Giannakakou P, et al. Paclitaxel-resistant human ovarian cancer cells have mutant beta-tubulins that exhibit impaired paclitaxel-driven polymerization. J Biol Chem. 1997;272(27):17118–25.
8. van Eijk M, et al. Cytochrome P450 3A4, 3A5, and 2C8 expression in breast, prostate, lung, endometrial, and ovarian tumors: relevance for resistance to taxanes. Cancer Chemother Pharmacol. 2019;84(3):487–99.
9. Asmarinah A, et al. Expression of the Bcl-2 family genes and complexes involved in the mitochondrial transport in prostate cancer cells. Int J Oncol. 2014;45(4):1489–96.
10. Calastretti A, et al. Down-modulation of Bcl-2 sensitizes PTEN-mutated prostate cancer cells to starvation and taxanes. Prostate. 2014;74(14):1411–22.
11. Puhr M, et al. Epithelial-to-mesenchymal transition leads to docetaxel resistance in prostate cancer and is mediated by reduced expression of miR-200c and miR-205. Am J Pathol. 2012;181(6):2188–201.
12. Roberts MS, et al. LIN9 and NEK2 are core regulators of mitotic fidelity that can be therapeutically targeted to overcome taxane resistance. Cancer Res. 2020;80(8):1693–706.
13. Zhang Z, et al. Downregulation of GPSM2 is associated with primary resistance to Paclitaxel in breast cancer. Oncol Rep. 2020;43(3):965–74.
14. Kopczynska E. Role of MicroRNAs in the resistance of prostate cancer to docetaxel and Paclitaxel. Contemp Oncol (Pozn). 2015;19(6):423–7.
15. Gremke N, et al. mTOR-mediated cancer drug resistance suppresses autophagy and generates a druggable metabolic vulnerability. Nat Commun. 2020;11(1):4684.
16. Guri Y, Hall MN. mTOR signaling confers resistance to targeted cancer drugs. Trends Cancer. 2016;2(11):688–97.
17. Ilagan E, Manning BD. Emerging role of mTOR in the response to cancer therapeutics. Trends Cancer. 2016;2(5):241–51.
18. Panner A, et al. mTOR controls FLIPS translation and TRAIL sensitivity in glioblastoma multiforme cells. Mol Cell Biol. 2005;25(20):8809–23.
19. Vanderweele DJ, Rudin CM. Mammalian target of Rapamycin promotes vincristine resistance through multiple mechanisms independent of maintained glycolytic rate. Mol Cancer Res. 2005;3(11):635–44.
20. Guertin DA, Sabatini DM. Defining the role of mTOR in cancer. Cancer Cell. 2007;12(1):9–22.
21. Tian T, Li X, Zhang J. mTOR signaling in cancer and mTOR inhibitors in solid tumor targeting therapy. Int J Mol Sci. 2019;20(3):755.
22. Faivre S, Kroemer G, Raymond E. Current development of mTOR inhibitors as anticancer agents. Nat Rev Drug Discov. 2006;5(8):671–88.
23. Murugan AK. mTOR: role in cancer, metastasis and drug resistance. Semin Cancer Biol. 2019;59:92–111.
24. Adhikari S, et al. The paradigm of drug resistance in cancer: an epigenetic perspective. Biosci Rep. 2022;42(4):BSR20211812.
25. Morel D, et al. Combining epigenetic drugs with other therapies for solid tumours - past lessons and future promise. Nat Rev Clin Oncol. 2020;17(2):91–107.
26. Singh D, Khan MA, Siddique HR. Role of epigenetic drugs in sensitizing cancers to anticancer therapies: emerging trends and clinical advancements. Epigenomics. 2023;15(8):517–37.
27. Huo H, et al. Histone methyltransferase MLL1 regulates MDR1 transcription and chemoresistance. Cancer Res. 2010;70(21):8726–35.
28. Li G, et al. Development of a dual targeting scaffold of SET7/MLL inhibitor for castration-resistant prostate cancer treatment. Genes Dis. 2023;10(6):2260–2.
29. Malik R, et al. Targeting the MLL complex in castration-resistant prostate cancer. Nat Med. 2015;21(4):344–52.
30. Yang L, Jin ML, Jeong KW. Histone H3K4 methyltransferases as targets for Drug-Resistant cancers. Biol Basel. 2021;10(7):581.
31. Gao SB, et al. The functional and mechanistic relatedness of EZH2 and Menin in hepatocellular carcinoma. J Hepatol. 2014;61(4):832–9.
32. Luo Y, et al. The scaffold protein Menin is essential for activating the MYC locus and MYC-mediated androgen receptor transcription in androgen receptor-dependent prostate cancer cells. Cancer Commun (Lond). 2021;41(12):1427–30.
33. Xu B, et al. Menin promotes hepatocellular carcinogenesis and epigenetically up-regulates Yap1 transcription. Proc Natl Acad Sci U S A. 2013;110(43):17480–5.
34. Yokoyama A, Cleary ML. Menin critically links MLL proteins with LEDGF on cancer-associated target genes. Cancer Cell. 2008;14(1):36–46.
35. Yokoyama A, et al. The Menin tumor suppressor protein is an essential oncogenic cofactor for MLL-associated leukemogenesis. Cell. 2005;123(2):207–18.
36. Cherif C, et al. Menin Inhibition suppresses castration-resistant prostate cancer and enhances chemosensitivity. Oncogene. 2022;41(1):125–37.
37. Kim T, et al. Menin enhances androgen Receptor-Independent proliferation and migration of prostate cancer cells. Mol Cells. 2022;45(4):202–15.

38. Fountzilas C, et al. COVALENT-102: A phase 1/1b dose finding study of BMF-219, an oral covalent Menin inhibitor, in adults with locally advanced, unresectable, or metastatic non-small cell lung cancer (NSCLC), pancreatic cancer (PDAC) and colorectal cancer (CRC) with activating KRAS mutations. J Clin Oncol. 2024;42(3suppl):TPS716–716.
39. Issa GC, et al. Menin Inhibition with revumenib for KMT2A-Rearranged relapsed or refractory acute leukemia (AUGMENT-101). J Clin Oncol. 2024;JCO2400826.43(1):75–84.
40. Diez-Villanueva A, Mallona I, Peinado MA. Wanderer, an interactive viewer to explore DNA methylation and gene expression data in human cancer. Epigenetics Chromatin. 2015;8:22.
41. Cerami E, et al. The cBio cancer genomics portal: an open platform for exploring multidimensional cancer genomics data. Cancer Discov. 2012;2(5):401–4.
42. Robinson D, et al. Integrative clinical genomics of advanced prostate cancer. Cell. 2015;162(2):454.
43. Jiang J, et al. CTR-DB 2.0: an updated cancer clinical transcriptome resource, expanding primary drug resistance and newly adding acquired resistance datasets and enhancing the discovery and validation of predictive biomarkers. Nucleic Acids Research. 2025;53(D1):D1335–47.
44. Lehmann BD, et al. Identification of human triple-negative breast cancer subtypes and preclinical models for selection of targeted therapies. J Clin Invest. 2011;121(7):2750–67.
45. Benchling [Biology Software]. Accessed: 15 July 2024. Available from: https://benchling.com
46. Ran FA, et al. Genome engineering using the CRISPR-Cas9 system. Nat Protoc. 2013;8(11):2281–308.
47. SRPlot. Available from: https://www.bioinformatics.com.cn/en. Accessed: 10 July 2024.
48. Eukaryotic Promoter. DataBase. Available from: https://epd.expasy.org/epd/ . Accessed: 20 June 2024.
49. NCBI. Primer Designing Tool. Accessed: 10 June 2024. Available from: https://www.ncbi.nlm.nih.gov/tools/primer-blast/
50. Sena G, et al. Measuring the complexity of cell cycle arrest and killing of drugs: kinetics of phase-specific effects induced by taxol. Cytometry. 1999;37(2):113–24.
51. So CW, Cleary ML. Common mechanism for oncogenic activation of MLL by forkhead family proteins. Blood. 2003;101(2):633–9.
52. Thomas LR, et al. Interaction of the oncoprotein transcription factor MYC with its chromatin cofactor WDR5 is essential for tumor maintenance. Proc Natl Acad Sci U S A. 2019;116(50):25260–8.
53. Chappell WH, et al. Influences of TP53 and the anti-aging DDR1 receptor in controlling Raf/MEK/ERK and PI3K/Akt expression and chemotherapeutic drug sensitivity in prostate cancer cell lines. Aging. 2020;12(11):10194–210.
54. ChIP Atlas Study, Study ID: SRX11712604. Available from: https://chip-atlas.org/view?id=SRX11712604. Accessed: 01 June 2024.
55. ChIP Atlas Study, Study ID: SRX14030471. Available from: https://chip-atlas.org/view?id=SRX14030471. Accessed: 01 June 2024.
56. ChIP Atlas Study, Study ID: SRX4046307. Accessed: 01 June 2024. Available from: https://chip-atlas.org/view?id=SRX4046307
57. ChIP Atlas Study, Study ID: SRX14030482. Available from: https://chip-atlas.org/view?id=SRX14030482. Accessed: 01 June 2024.
58. ChIP Atlas Study, Study ID: SRX11712606. Available from: https://chip-atlas.org/view?id=SRX11712606. Accessed: 01 June 2024.
59. Goel S, et al. Overcoming therapeutic resistance in HER2-Positive breast cancers with CDK4/6 inhibitors. Cancer Cell. 2016;29(3):255–69.
60. VanArsdale T, et al. Molecular pathways: targeting the Cyclin D-CDK4/6 axis for cancer treatment. Clin Cancer Res. 2015;21(13):2905–10.
61. Hume S, Dianov GL, Ramadan K. A unified model for the G1/S cell cycle transition. Nucleic Acids Res. 2020;48(22):12483–501.
62. Daksis JI, et al. Myc induces Cyclin D1 expression in the absence of de Novo protein synthesis and links mitogen-stimulated signal transduction to the cell cycle. Oncogene. 1994;9(12):3635–45.
63. Wu G, et al. Menin enhances c-Myc-mediated transcription to promote cancer progression. Nat Commun. 2017;8:15278.
64. Ng SS, et al. Cell cycle-related kinase: a novel candidate oncogene in human glioblastoma. J Natl Cancer Inst. 2007;99(12):936–48.
65. Tian Y, Wan H, Tan G. Cell cycle-related kinase in carcinogenesis. Oncol Lett. 2012;4(4):601–6.
66. Wu GQ, et al. Cell cycle-related kinase supports ovarian carcinoma cell proliferation via regulation of Cyclin D1 and is a predictor of outcome in patients with ovarian carcinoma. Int J Cancer. 2009;125(11):2631–42.
67. Mansoori B, et al. The different mechanisms of cancer drug resistance: A brief review. Adv Pharm Bull. 2017;7(3):339–48.
68. Yu X, et al. Cancer epigenetics: from laboratory studies and clinical trials to precision medicine. Cell Death Discov. 2024;10(1):28.
69. Daver N, et al. Phase 1/2 First-in-Human study of the Menin-MLL inhibitor DSP-5336 in patients with relapsed or refractory acute leukemia. Blood. 2023;142:2911 .
70. Grembecka J, et al. Menin-MLL inhibitors reverse oncogenic activity of MLL fusion proteins in leukemia. Nat Chem Biol. 2012;8(3):277–84.
71. Lei H, et al. Recent progress of small molecule Menin-MLL interaction inhibitors as therapeutic agents for acute leukemia. J Med Chem. 2021;64(21):15519–33.
72. Ye J, et al. Co-inhibition of HDAC and MLL-menin interaction targets MLL-rearranged acute myeloid leukemia cells via disruption of DNA damage checkpoint and DNA repair. Clin Epigenetics. 2019;11(1):137.
73. Chandrasekharappa SC, et al. Positional cloning of the gene for multiple endocrine neoplasia-type 1. Science. 1997;276(5311):404–7.
74. Suzuki J, et al. The tumor suppressor Menin prevents effector CD8 T-cell dysfunction by targeting mTORC1-dependent metabolic activation. Nat Commun. 2018;9(1):3296.
75. Braun KA, et al. Menin drives oncogenesis in ewing sarcoma cells by activating transcription of key metastatic factors. Cancer Res. 2024;84(6):6601-6601 .
76. Dreijerink KMA, Timmers HTM, Brown M. Twenty years of menin: emerging opportunities for restoration of transcriptional regulation in MEN1. Endocr Relat Cancer. 2017;24(10):T135–45.
77. Wang ZF, et al. Abnormal expression of Menin predicts the pathogenesis and poor prognosis of adult gliomas. Cancer Gene Ther. 2020;27(7–8):539–47.
78. Feng Z, Ma J, Hua X. Epigenetic regulation by the Menin pathway. Endocr Relat Cancer. 2017;24(10):T147–59.
79. Bitting RL, Armstrong AJ. Targeting the PI3K/Akt/mTOR pathway in castration-resistant prostate cancer. Endocr Relat Cancer. 2013;20(3):R83–99.
80. Dong C, et al. Activation of PI3K/AKT/mTOR pathway causes drug resistance in breast cancer. Front Pharmacol. 2021;12:628690.
81. Edlind MP, Hsieh AC. PI3K-AKT-mTOR signaling in prostate cancer progression and androgen deprivation therapy resistance. Asian J Androl. 2014;16(3):378–86.
82. Faruq O, et al. Targeting an MDM2/MYC axis to overcome drug resistance in multiple myeloma. Cancers (Basel). 2022;14(6):1592.
83. Jiang BH, Liu LZ. Role of mTOR in anticancer drug resistance: perspectives for improved drug treatment. Drug Resist Updat. 2008;11(3):63–76.
84. Pungsrinont T, Kallenbach J, Baniahmad A. Role of PI3K-AKT-mTOR pathway as a Pro-Survival signaling and Resistance-Mediating mechanism to therapy of prostate cancer. Int J Mol Sci. 2021;22(20):11088.
85. Xia B, et al. c-Myc plays part in drug resistance mediated by bone marrow stromal cells in acute myeloid leukemia. Leuk Res. 2015;39(1):92–9.
86. Xie C, et al. C-Myc participates in beta-catenin-mediated drug resistance in A549/DDP lung adenocarcinoma cells. APMIS. 2014;122(12):1251–8.
87. Armstrong AJ, et al. A phase II trial of Temsirolimus in men with castration-resistant metastatic prostate cancer. Clin Genitourin Cancer. 2013;11(4):397–406.
88. Massague J. G1 cell-cycle control and cancer. Nature. 2004;432(7015):298–306.
89. Montalto FI, De Amicis F. Cyclin D1 in cancer: a molecular connection for cell cycle Control, adhesion and invasion in tumor and stroma. Cells. 2020;9(12):2648.
90. Feng H, et al. A CCRK-EZH2 epigenetic circuitry drives hepatocarcinogenesis and associates with tumor recurrence and poor survival of patients. J Hepatol. 2015;62(5):1100–11.
91. Yang Y, Roine N, Makela TP. CCRK depletion inhibits glioblastoma cell proliferation in a cilium-dependent manner. EMBO Rep. 2013;14(8):741–7.

Publisher's note

Springer Nature remains neutral with regard to jurisdictional claims in published maps and institutional affiliations.